Front. Phys. China, 2007, 2(2): 171−177
DOI 10.1007/s11467-007-0032-5

REVIEW ARTICLE

LIU Hui-jun

Interaction of oxygen with 4 Å carbon nanotubes

Abstract We review our density functional study of oxygen adsorption on the outer surface of 4 Å single-wall carbon nanotubes, which have been recently synthesized using a templating method. The stability of these 4 Å tubes under ambient conditions is investigated by the nudged elastic band technique and further confirmed by the experimentally measured Raman spectra. Different adsorption pictures of singlet O_2 could be used to select a single chirality from a mixture of these ultra-small radius tubes.

Keywords density functional theory, carbon nanotubes, oxygen adsorption, reaction path

PACS numbers 71.20.Tx, 71.15.Mb, 73.22.-f, 61.46.Fg

1 Introduction

In the past decade, carbon nanotubes have attracted a lot of attention from the science community due to their interesting novel properties and great application in nanotechnology [1−3]. Among them, single-wall carbon nanotubes (SWNTs) are of particular importance and their quasi-one-dimensional characteristics have been intensively investigated. However, the synthesis of SWNTs is challenging, especially for SNWTs with very small diameters. Recently, ultrasmall SWNTs have been successfully fabricated inside the confined environment of inert $AlPO_4$–5 zeolite (AFI) channels [4−7]. These nanotubes are perfectly aligned with a diameter of about 4 Å, probably at or close to the theoretical limit. The large curvature gives them many unusual properties such as superconducting fluctuations [8], high Li storage capacity [9], and efficient visible photoluminescence [10], etc.

Recently, there is a growing interest in gas adsorption by carbon nanotubes [11−20]. Among them, the interactions of oxygen with SWNTs are widely studied. Experimentally, it has been shown that the electronic and transport properties of carbon nanotubes are extremely sensitive to oxygen exposure [14−16]. One obvious application of such sensitivity is the construction of gas sensors built from SWNTs. On the theoretical side, many calculations and analyses with different levels of sophistication have been reported [20−35]. Some of these studies are focused on the physisorption of O_2 while others consider both physisorption and chemisorption. Various adsorption sites, both inside and outside of SWNTs are discussed and compared with each other and also with graphene. Although some conclusions are similar, there are also several controversial results about the oxygen binding energies, the equilibrium binding distance between oxygen and tube, and whether the reaction is exothermic or endothermic.

To date, most of these works are focused on the zigzag and armchair SWNTs with relatively larger diameters. To the best of our knowledge, there is no theoretical study on the oxygen adsorption of ultrasmall (~ 4 Å in diameter) SWNTs and in particular, the effect of chirality, which is expected to be stronger in smaller diameter tubes. There are actually three types of SWNTs with a diameter of about 4 Å, namely, the zigzag (5, 0), the armchair (3, 3), and the chiral (4, 2). Evidence from Raman spectra and optical absorption suggest that all of them co-exist inside the AFI zeolite channels [7, 36, 37], and the AFI can be dissolved by acid to recover them as standalone entities. Due to the large curvature, these ultra-small tubes are expected to be more reactive than larger-diameter tubes, and thus whether they are air stable is an issue that needs to be addressed. In this review, we summarize our recent density functional study of oxygen adsorption on the outer surface of these 4 Å nanotubes. Our aim is to investigate whether these tubes are stable (and if so, how stable) when they are exposed in ambient conditions. Here

LIU Hui-jun (✉)
Department of Physics and Key Laboratory of Acoustic and Photonic Materials and Devices (Ministry of Education), Wuhan University, Wuhan 430072, China
E-mail: phlhj@whu.edu.cn

Received February 9, 2007

we only consider the singlet $O_2(^1\Delta_g^+)$ since it is much more reactive than the triplet state $(^3\Sigma_g^-)$ and is mainly responsible for the oxidation [24].

2 Computational details

Our total energy calculations were performed using a plane-wave pseudopotential method, as implemented in the Vienna Ab-initio Simulation Package (VASP) [38−40]. The exchange-correlation energy is in the form of Perdew-Wang-91 [41], and the cutoff energy is 396 eV for the plane wave basis set. A standard hexagonal supercell is used to model the carbon nanotubes and the adsorbed oxygen. The center-to-center distance between adjacent tubes in the supercell is 16 Å, which allows for negligible interaction between the tubes (together with the adsorbed oxygen) and its periodic images. The ***k***-points are sampled on a uniform grid along the tube axis, and atomic positions are fully relaxed. To calculate the energy barriers involved in the reaction process, we use the so-called nudged elastic band (NEB) method [42, 43]. The NEB is an efficient method for finding saddle points and minimum energy paths (MEP) between a given initial and final state of a reaction. In our calculations, a number of intermediate images of the system (typically on the order of 8) are constructed along the reaction path, and each image finds the lowest energy while maintaining equal spacing to neighboring images. This constrained optimization is done by adding spring forces along the band between images and by projecting out the component of the forces due to the potential perpendicular to the band. To drive the highest energy image exactly to the saddle point, the climbing image [44] is used after the regular NEB.

3 Adsorption picture

For tubes (5, 0) and (3, 3), there are two different adsorption sites of oxygen on the outer surface. One site (I) is related to the carbon-carbon bonds that are aligned "along" the tube axis, and the other (II) is associated with the bonds that are wrapping "around" the tube circumference. These adsorption sites are schematically shown in Fig. 1. As for tube (4, 2), it has three inequivalent C−C bonds and thus offers three distinct adsorption sites marked as A, B and C in Fig. 1.

3.1 Zigzag (5, 0)

We first focus on the zigzag (5, 0). We find that physisorption of O_2 occurs on both site I and site II, but the binding is very weak and at the margin of the accuracy of DFT calculations (Table 1). This is consistent with the fact that the O–O distance in the physisorbed product is very close to the bond length in the free O_2 molecule, and that the tube's geometry is almost unchanged. We want to mention that singlet O_2 physisorbs on site I at a distance of 3.43 Å with a binding energy of about –0.08 eV. This energy value is considerably smaller than those found in previous theoretical studies for bigger tubes [21, 45]. We believe that this discrepancy is mainly due to the use of LDA in previous calculations while we use GGA. The LDA is known to overestimate binding energies. The equilibrium O_2−tube distance by our GGA calculations is also larger than the LDA value of 2.7 Å. Our results agree well with those obtained for O_2 physisorbed on the bridged site of (8,0), where the GGA was used in the calculations [31]. As for chemisorption, we find a quite different picture. The O_2 molecule binds strongly on both sites. In the case of site I, two C−O bonds are formed making a "square" ring shown as a ball-and-stick model in Fig. 2 below. The tube's geometry is significantly modified due to the strong interaction between the O_2 molecule and the tube. The O_2 molecule bond (parallel to the tube axis) is not broken, although the O−O distance is larger than that of the free O_2 molecule. This is also the case of site II except that the O−O bond is not parallel to the underlying C−C bond, as shown in Fig. 3 below. Such adsorption of singlet O_2 is known as

Table 1 Calculated binding energy (in unit of eV) and O−O bond length (in unit of Å) for singlet O_2 adsorbed on tube (5, 0). The zero of the energy is defined as the total energy of a pristine tube plus a singlet O_2.

Tube (5, 0)	E_b	O−O
Physisorption (site I)	−0.08	1.249
Physisorption (site II)	−0.19	1.253
Chemisorption (site I)	−1.63	1.511
Chemisorption (cyclo)	−1.06	1.512
Chemisorption (epoxy)	−3.06	3.197

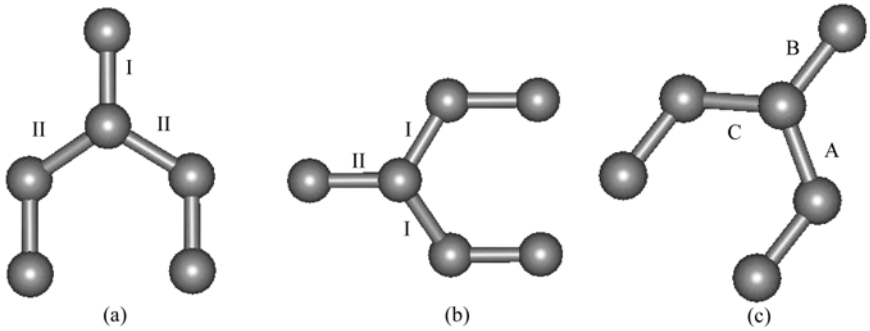

Fig. 1 Distinct adsorption sites of oxygen on the outer surface of **(a)** (5,0), **(b)** (3,3) and **(c)** (4,2).

cyclo-addition. Besides these two chemisorbed products, we find a more stable epoxy structure with the dissociation of O_2 and each O atom taking site I (also see Fig. 3 below). The calculated binding energy for epoxy is −3.06 eV relative to singlet O_2.

Figure 2 shows the NEB calculated minimum energy path from physisorption (site I) to chemisorption (site I), where the average C−O distance is taken as the reaction coordinate. Relative to the physisorbed product, the chemisorbed product is 1.55 eV lower in energy. The activation barrier is only 0.30 eV, which means that (5, 0) tube can be easily oxidized in ambient environment. The reaction path is similar to those previously found for larger zigzag tubes (8,0), except that the energy barrier is quite a bit smaller than the reported value of 0.75 eV [24, 46]. This means that our 4 Å tube is more reactive than larger diameter tubes.

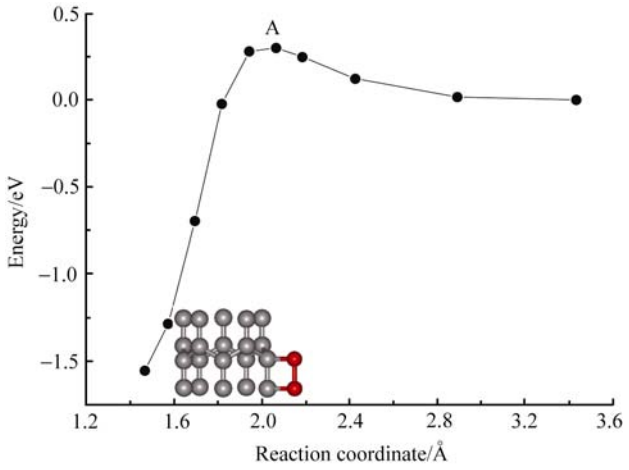

Fig. 2 The minimum energy path from physisorption (site I) to chemisorption (site I) of singlet O_2 on tube (5, 0). The energy of physisorbed product is set at zero.

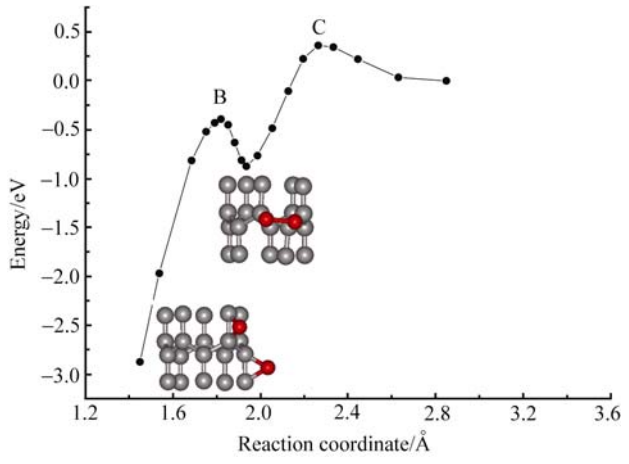

Fig. 3 The minimum energy path from physisorption (site II) to the cyclo-addition and epoxy state of singlet O_2 on tube (5, 0). The energy of physisorbed product is set at zero.

The reaction path from physisorption (site II) to cyclo-addition product is shown in Fig. 3. Relative to the physisorbed product, the cyclo-addition structure is 0.87 eV more stable. As shown in Fig. 3, the activation barrier is also quite low with a value of 0.36 eV. The cyclo-addition product could go another step to the more stable epoxy product, with an energy barrier of 0.48 eV. A similar reaction pathway was first shown in Ref. [24] for larger tubes (8, 0). However, for our ultra-small tube (5, 0), the activation barriers are lower than those found for (8, 0) (the values are 0.61 eV and 0.54 eV, respectively), and again this means that the (5, 0) tube is not stable when exposed to oxygen. We want to mention that once the epoxy structure is formed, the desorption barrier becomes 2.48 eV and that is quite high. It is thus difficult in experiment to completely get rid of the adsorbed O_2.

3.2 Armchair (3, 3)

The adsorption properties of O_2 on the armchair (3, 3) are summarized in Table 2. The small energy values listed in the first two rows are characteristics of physisorption, and the corresponding O−O bond length is only slightly larger than that of a free O_2 molecule. For the chemisorption of O_2 on site II, there is a dramatic change of the tube's geometry, which is not found in zigzag (5, 0). As before, two C−O bonds are formed; however, one of the C−C bond is now broken which means that the tube's structure will be destroyed upon such adsorption (see Fig. 4 below). The epoxy structure, with each O atom occupying site II, has the lowest energy and the opening of C−C bond is also observed (see Fig. 5 below). The chemisorbed product with energy in between is the cyclo-addition of O_2 on top of site I, as also shown in Fig. 5.

Table 2 Calculated binding energy (in unit of eV) and O−O bond length (in unit of Å) for singlet O_2 adsorbed on tube (3,3). The zero of the energy is defined as the total energy of a pristine tube plus a singlet O_2.

Tube (3, 3)	E_b	O−O
Physisorption (site I)	−0.21	1.261
Physisorption (site II)	−0.27	1.265
Chemisorption (site II)	−3.43	2.727
Chemisorption (cyclo)	−1.07	1.525
Chemisorption (epoxy)	−4.19	3.604

Figure 4 shows the calculated MEP from physisorption to chemisorptions at site II. Relative to the physisorbed state, the chemisorbed product is much lower in energy, but the activation barrier is only 0.35 eV. The reaction path from physisorption to cyclo-addition of O_2 on (3, 3) is given in Fig. 5. We see that the energy barrier is quite small with a value of 0.21 eV, which means that tube (3, 3) is even more reactive than tube (5, 0). This is also consistent with the fact that tube (3, 3) has the largest curvature of C−C bond on the tube's wall among the three types of 4 Å tubes. We may ex-

pect that the cyclo-addition product could go through another step to the epoxy state, as the case previously reported for large armchair tube (6, 6) [24, 46]. However, during our NEB calculations, we find another chemisorbed state between the cyclo-addition and epoxy products. A ball-and-stick model of this intermediate state is also shown in Fig. 5. We see that the O_2 is dissociated and the underlying C–C bond is broken; the tube's geometry is dramatically changed due to the strong interaction between the tube and oxygen.

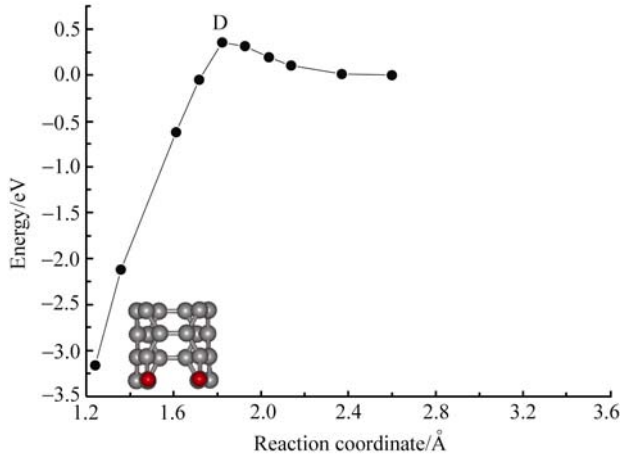

Fig. 4 The minimum energy path from physisorption to chemisorption of singlet O_2 on tube (3, 3) at site II. The energy of physisorbed product is set at zero.

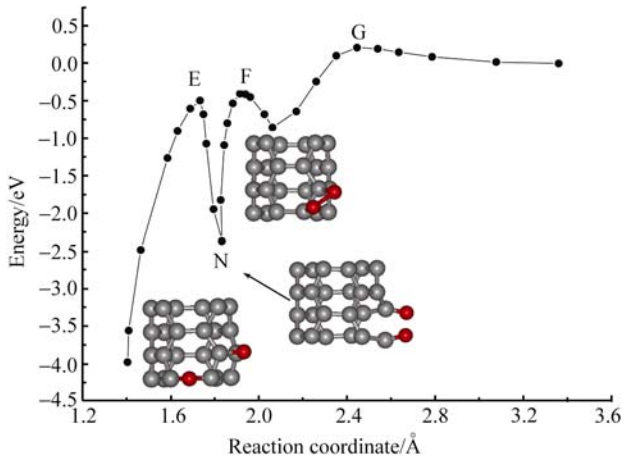

Fig. 5 The minimum energy path from physisorption to the cyclo-addition and epoxy state of singlet O_2 on tube (3, 3). An intermediate chemisorbed state is found between them. The energy of the physisorbed product is set at zero.

As shown in Fig. 5, this new chemisorbed state is lower in energy than the cyclo-addition state but higher than the epoxy state. The presence of the intermediate state makes the reaction path quite different from that reported before for larger armchair tube (6, 6). The energy barrier is 0.46 eV from the cyclo-addition product to this intermediate state, and 1.87 eV from the intermediate state to the epoxy state. Since the latter is so high, the probability of reaching the epoxy configuration is small under ambient conditions, and the intermediate will be the main oxidation product. More importantly, once reaching the intermediate state, the desorption barrier becomes 1.96 eV, which means that it will be difficult to completely clean the adsorbed oxygen when such a structure is present.

3.3 Chiral (4, 2)

The adsorption picture for the chiral (4, 2) tube is a bit complex since it has three distinct adsorption sites as shown in Fig. 1. We first focus on site A, which has the smallest angle with the tube axis. We find that physisorption occurs at a distance of about 3.16 Å with a binding energy of 0.11 eV. As for the chemisorption, we find that two C–O bonds are formed and the O–O bond is elongated but still kept. The underlying C–C bond length also increases by about 0.11 Å. Such adsorption of singlet O_2 is known as cycloaddition. The calculated binding energy is 1.30 eV and the tube's geometry is modified due to the strong interaction between the O_2 molecule and the (4, 2) tube. Figure 6 gives the NEB calculated minimum-energy path from physisorption to chemisorption for site A, where a ball-and-stick model of the chemisorbed product is also shown. Relative to the physisorbed product, the chemisorbed product is 1.19 eV more stable. The energy barrier from physisorption to chemisorption is found to be 0.52 eV, which is slightly higher than those of (5, 0) and (3, 3) tubes but obviously lower than previously reported for larger-diameter tubes. This indicates that these ultra-small tubes are more reactive than larger-diameter tubes. For very large tube, it is more like a flat graphene sheet in terms of reactivity, and the chemisorption of O_2 will be more difficult [24]. A more detailed discussion on the dependence of tube diameter can be found in reference [47]. Of course, the adsorption behavior as well as the electronic structure will also depend on the chirality of corresponding nanotubes. The calculated structural parameters for the physisorbed, the chemisorbed, and the transition states are summarized in Table 3.

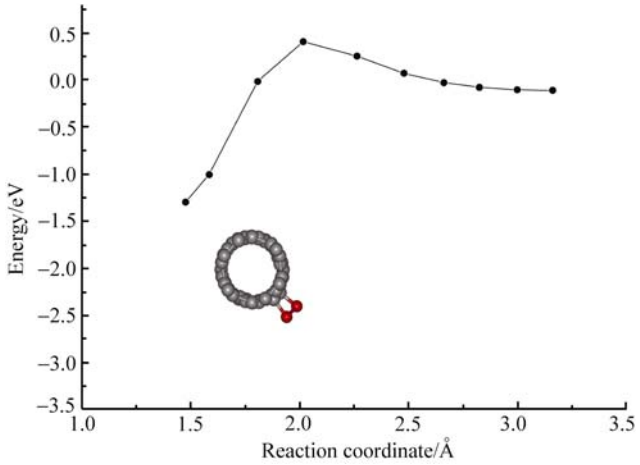

Fig. 6 The minimum-energy path from physisorption to chemisorption of O_2 on the site A of (4, 2) tube, where the zero of energy is set as the total energy of pristine (4, 2) and free O_2.

Table 3 Calculated structural parameters for three different physisorbed states (PS), chemisorbed states (CS) and transition states (TS) in (4,2) tube. $R_{O\text{-}O}$ is the O−O distance. $R_{C-O}(1)$ and $R_{C-O}(2)$ are the distance from each O atom to the nearest C atom. $R_{C-C}(1)$ is the underlying C−C distance, and $R_{C\text{-}C}(2)$ and $R_{C\text{-}C}(3)$ are the two nearby C−C distance. The unit is Å.

	PS (A)	TS (A)	CS (A)	PS (B)	TS (B)	CS (B)	PS (C)	TS (C)	CS (C)
R_{O-O}	1.256	1.315	1.520	1.259	1.344	1.520	1.257	1.331	2.790
$R_{C-O}(1)$	3.144	2.003	1.475	2.602	1.861	1.487	3.127	1.910	1.237
$R_{C-O}(2)$	3.179	2.029	1.476	2.649	1.907	1.489	3.114	1.913	1.238
$R_{C-C}(1)$	1.419	1.489	1.533	1.420	1.442	1.493	1.419	1.438	1.477
$R_{C-C}(2)$	1.437	1.440	1.525	1.440	1.443	1.504	1.438	1.536	2.810
$R_{C-C}(3)$	1.440	1.454	1.508	1.443	1.509	1.560	1.441	1.446	1.473

We next consider adsorption on site B, which has a larger angle with the tube axis. Compared with that for site A, we find that the physisorption occurs at a closer tube–O_2 distance (2.63 Å). As a result, the binding energy (0.20 eV) is also a bit larger. The calculated O−O distance is still 1.26 Å and the tube's structure is almost unchanged due to weak tube–O_2 interaction. Chemisorption on site B is also cycloaddition; however, the binding energy is only 0.72 eV and the tube's geometry is slightly modified. Due to the curvature effect, the C−C distance on site B is a bit larger than that on site A, which means that site B is more reactive. In Fig. 7, we show the NEB calculated minimum-energy path from the physisorbed state to the chemisorbed state for site B. The energy barrier of 0.45 eV is slightly lower than the case of site A, which again indicates that site B is more reactive.

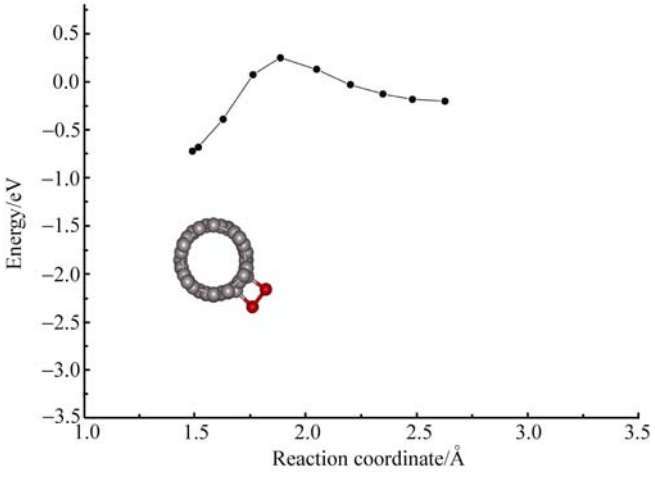

Fig. 7 The minimum-energy path from physisorption to chemisorption of O_2 on the site B of (4, 2) tube, where the zero of energy is set as the total energy of pristine (4, 2) and free O_2.

Among the three distinct adsorption sites, site C has the largest angle with the tube axis. As before, the physisorbed product has a small binding energy of 0.15 eV. However, the chemisorbed state is much lower in energy and the adsorption is no longer cycloaddition-like. We find that O_2 is dissociated and the underlying C−C bond is broken, very similar to those found for (3,3) tube. The calculated binding energy is 3.17 eV, and the tube's geometry is significantly changed as can also be seen from Table 3. All these indicate that there is a very strong interaction between the tube and oxygen. We have also calculated the minimum-energy path from physisorbed product to chemisorbed state for site C and find that the energy barrier is even smaller (0.42 eV). The results are shown in Fig. 8. It is interesting to note that due to the curvature effect, site C is more reactive than site A, with site B in between. According to our NEB calculation, site C has the lowest energy barrier for reaction with O_2, while site A the highest and site B is also in between. Both of these findings suggest that upon oxygen exposure, (4, 2) tube will be oxidized firstly from site C. Once such oxidation occurs and the chemisorbed product is formed, the (4, 2) tube will be destroyed as characterized by the broken C−C bond and significant change of tube's geometry. This is however not the case for (5, 0) tube as we just discussed. The geometry of (5, 0) tube is still kept when exposed to oxygen, which indicates that (5, 0) tube is more stable than (4, 2) tube in ambient conditions. As we knew, the as-grown product of 4 Å SWNTs usually contains a mixture of (5, 0), (4, 2) and (3, 3). The different adsorption picture of O_2 suggests that we can use oxidation to select a single chirality from these three kinds of tubes.

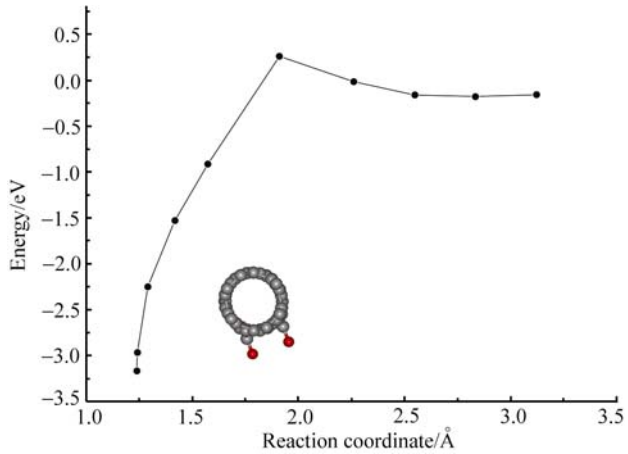

Fig. 8 The minimum-energy path from physisorption to chemisorption of O_2 on the site C of (4, 2) tube, where the zero of energy is set as the total energy of pristine (4, 2) and free O_2.

4 Raman spectra

The difference in the air stability of (4, 2) and (5, 0) tubes can also be found by investigation of their Raman spectra. Figure 9(a) gives the measured Raman spectra of these 4 Å SWNTs for various temperatures. The nanotubes were confined in the channels of AFI crystals and treated under the vacuum of 10^{-3} mbar. Since this is not a high vacuum condition, and considering the fact that the energy barriers from physisorption to chemisorption for these 4 Å SWNTs are quite small, we cannot rule out oxidation in the experimental measurement. As can be seen from Fig. 9(a), the Raman spectra exhibit three main features: (1) In the low frequency region (see inset), the Raman lines at 510 cm^{-1} and 550 cm^{-1} are attributed to the radial breathing mode (RBM) of (4, 2) and the (5, 0) tubes, respectively [48]. The RBM signal of (3, 3) tube is very weak because the excitation wavelength is off-resonance for the sample; (2) The D bands in the intermediate region (1200−1500 cm^{-1}) are characteristic of a disorder structure; (3) The tangential G bands in the high frequency region (1500−1620 cm^{-1}) are characteristic of carbon bond vibration. Since RBM is specific to the cylindrical geometry of nanotubes, while G-band is a common feature for all carbon materials (except diamond), it is straightforward to say more carbon nanotubes are oxidized when the relative intensity of RBM is decreased. In the low frequency region, we see that the intensity of RBM at 510 cm^{-1} weakens with increasing temperature, and finally becomes undetectable at a temperature of 1273 K, which is a direct indication of structure collapse caused by oxidation. In contrast, the RBM at 550 cm^{-1} survives up to 1273 K. All these results suggest that among the two types of the 4 Å SWNTs, the (5, 0) tube with zigzag structure is more air stable than the (4, 2) tube with chiral structure. The (4, 2) tube is obviously oxidized around 1123 K, while the (5, 0) tube is still air stable up to 1273 K. On the other hand, the relative intensity of D bands in the intermediate frequency region increases with increasing temperature. This can be attributed to the fact that the concentration of oxygen is very low, thus the reaction rate between nanotubes and oxygen is slow, which leads to the collapse of nanotubes and turning into amorphous carbon because of the large curvature. The structure collapse is accelerated with increasing temperature. Isothermal Raman spectra shown in Fig. 9b are measured by keeping the temperature at 1123 K for various duration times. We see that the RBM feature of (4, 2) tube disappears gradually with increasing duration time, implying that the (4, 2) tube structure is slowly destroyed by oxidation. The slight increase of the relative intensity of D bands is also an indication of structural destruction. However, the RBM feature of (5, 0) tube is still observable even after 50 hours, which again indicates that (5, 0) tube is more stable than (4, 2) tube in the sense of oxidation. The experimental observation is consistent with our theoretical predication.

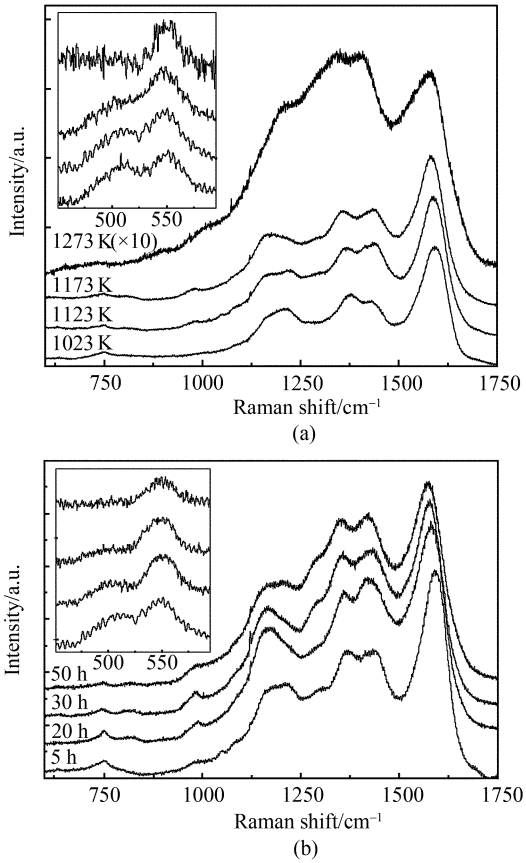

Fig. 9 Measured Raman spectra of 4 Å SWNT treated **(a)** at various temperatures, and **(b)** at various duration times. The inset shows the magnified spectra around RBM.

5 Summary

In summary, we have studied interaction of the O_2 molecule with the 4 Å SWNTs by density functional calculations. The NEB calculated minimum-energy path from physisorption to chemisorption are discussed in detail and compared with other larger diameter tubes. The chirality plays a very important role in the oxygen binding energy and the reaction process. Our theoretical calculations and experimentally measured Raman spectra both indicate that (4, 2) tube is not more air stable than (5, 0) tube, which could be used to select a single chirality from a mixture of these 4 Å tubes.

Acknowledgements We thank Prof. C.T. Chan, Prof. Ping Sheng, Prof. Z. K. Tang and Dr. J. P. Zhai at the Hong Kong University of Science and Technology for many helpful discussions. This work was supported by the National Natural Science Foundation of China (Grant No. 10504025) and the Natural Science Foundation of Hubei Province (Grant No. 2005ABA035).

References

1. Eletskiĭ A.V., Physics-Uspekhi, 1997, 40: 899

2. Saito R., Dresselhaus G., and Dresselhaus M. S., Physical Properties of Carbon Nanotubes, London: Imperial College Press, 1998
3. Reich S., Thomsen C., and Maultzsch J., Carbon Nanotubes: Basic Concepts and Physical Properties, Cambridge: Wiley-VCH, 2004
4. Sun H.D., Tang Z.K., Chen J.S., and Li G.D., Solid State Comm., 1999, 109: 365
5. Tang Z. K., Sun H. D., Wang J., Chen J. S., and Li G. D., Appl. Phys. Lett., 1998, 73: 2287
6. Sun H.D., Tang Z. K., Chen J. S., and Li G. D., Appl. Phys. A, 1999, 69: 381
7. Wang N., Tang Z. K., Li G. D., and Chen J. S., Nature, 2000, 408: 51
8. Tang Z.K., Zhang L. G., Wang N., Zhang X.X., Wen G. H., Li G. D., Wang J. N., Chan C.T., and Sheng P., Science, 2001, 292: 2467
9. Liu H. J., Li Z. M., Liang Q., Tang Z. K., and Chan C. T., Appl. Phys. Lett., 2004, 84: 2649
10. Guo J. D., Yang C. L., Li Z. M., Bai M., Liu H. J., Li G. D., Wang E. G., Chan C. T., Tang Z. K., Ge W. K., and Xiao X. D., Phys. Rev. Lett., 2004, 93: 017402
11. Dillon A.C., Jones K. M., Bekkdeahl T. A., Kiang C. H., Bethune D. S., and Heben M.J., Nature (London) , 1997, 386: 377
12. Gadd G. E., Blackford M., Moricca S., Webb N., Evans P. J., Smith A. M., Jacobsen G., Leung S., Day A., and Hua Q., Science, 1997, 277: 933
13. Dean K. A. and Chalamala B. R., Appl. Phys. Lett., 1999, 75: 3017
14. Kong J., Franklin N. R., Zhou C. C., Chapline M, G., Peng S., Cho K. J., and Dai H. J., Science, 2000, 287: 622
15. Collins P. G., Bradley K., Ishigami M., and Zettl A., Science, 2000, 287: 1801
16. Tang X. P., Kleinhammes A., Shimoda H., Fleming L., K. Bennoune Y., Sinha S., Bower C., Zhou O., and Wu Y., Science, 2000, 288: 492
17. Sumanasekera G. U., Adu C. K. W., Fang S., and Eklund P. C., Phys. Rev. Lett., 2000, 85: 1096
18. Fujiwara A., Ishiia K., Suematsua H., Kataurab H., Maniwab Y., Suzukic S., and Achibac Y., Chem. Phys. Lett., 2001, 336: 205
19. Wadhawan A., Stallcup R. E. II, and Perez J. M., Appl. Phys. Lett., 2001, 78: 108
20. Zhao J., Buldum A., Han J., and Lu J. P., Nanotechnology, 2002, 13: 195
21. Jhi S. H., Louie S. G., and Cohen M. L., Phys. Rev. Lett., 2000, 85: 1710
22. Zhu X. Y., Lee S. M., Lee Y. H., and Frauenheim T., Phys. Rev. Lett., 2000, 85: 2757
23. Bradley K., Jhi S. H., Collins P. G., Hone J., Cohen M. L., Louie S.G., and Zettl A., Phys. Rev. Lett., 2000, 85: 4361
24. Chan S. P., Chen G., Gong X. G., and Liu Z.F., Phys. Rev. Lett., 2003, 90: 086403−1
25. Park N., Han S.W., and Ihm J., Phys. Rev. B, 2001, 64: 125401
26. Moon C.Y., Kim Y. S., Lee E. C., Jin Y. G., and Chang K. J., Phys. Rev. B, 2002, 65: 155401
27. Dag S., Gülseren O., Yildirim T., and Ciraci S., Phys. Rev. B, 2003, 67: 165424
28. Ricca A., Bauschlicher C. W., and Maiti A., Phys. Rev. B, 2003, 68: 035433
29. Froudakis G. E., Schnell M., Muhlhauser M., Peyerimhoff S.D., Andriotis A. N., Menou M., and Sheetz R. M., Phys. Rev. B, 2003, 68: 115435
30. Miyake T. and Satio S., Phys. Rev. B, 2003, 68: 155424
31. Sorescu D. C., Jordan K. D., and Avouris P., J. Phys. Chem. B, 2001, 105: 11227
32. Mann D. J. and Halls M. D., Chem J.. Phys., 2002, 116: 9014
33. Dag S., Gülseren O., and Ciraci S., Chem. Phys. Lett. B, 2003, 380: 1
34. Giannozzi P., Car R., and Scoles G., Chem J.. Phys., 2003, 118: 1003
35. Barone V., Heyd J., and Scuseria G. E., Chem. Phys. Lett., 2004, 389: 289
36. Li Z. M., Tang Z. K., Liu H. J., Wang N., Chan C. T., Saito R., Okada S., Li G.D., Chen J. S., Nagasawa N., and Tsuda S., Phys. Rev. Lett., 2001, 87: 127401−1
37. Liu H. J. and Chan C. T., Phys. Rev. B, 2002, 66: 115416
38. Kresse G. and Hafner J., Phys. Rev. B, 1993, 47: 558
39. Kresse G. and Hafner J., Phys. Rev. B, 1994, 49: 14251
40. Kresse G. and Furthmüller J., Comput. Mat. Sci., 1996, 6: 15
41. Perdew J. P. and Wang Y., Phys. Rev. B, 1992, 45: 13244
42. Jonsson H., Mills G., Jacobsen K. W., Nudged Elastic Band Method for Finding Minimum Energy Paths of Transitions, in Classical and Quantum Dynamics in Condensed Phase Simulations, Edited by B. J. Berne, G. Ciccotti and D. F. Coker ,World Scientific, 1998: 385
43. Henkelman G. and Jonsson H., Chem J.. Phys., 2000, 113: 9978
44. Henkelman G., Uberuaga B. P., and Jonsson H., Chem J.. Phys., 2000, 113: 9901
45. Peng S. and Cho K., Nanotechnology, 2000, 11: 57
46. Chan S. P., PhD thesis, The Chinese University of Hong Kong., 2004
47. Zhang Y. F. and Liu Z. F., J. Phys. Chem. B, 2004, 108: 11435
48. Li Z. M., Liu H. J., Ye J. T., Chan C. T., and Tang Z. K., Appl. Phys. A , 2004, 78: 1121